nature neuroscience

Mutant Huntingtin promotes autonomous microglia activation via myeloid lineage-determining factors

Andrea Crotti[1], Christopher Benner[2], Bilal E Kerman[3], David Gosselin[1], Clotilde Lagier-Tourenne[4,5], Chiara Zuccato[6], Elena Cattaneo[6], Fred H Gage[3], Don W Cleveland[1,5] & Christopher K Glass[1,7]

Huntington's disease (HD) is a fatal neurodegenerative disorder caused by an extended polyglutamine repeat in the N terminus of the Huntingtin protein (HTT). Reactive microglia and elevated cytokine levels are observed in the brains of HD patients, but the extent to which neuroinflammation results from extrinsic or cell-autonomous mechanisms in microglia is unknown. Using genome-wide approaches, we found that expression of mutant Huntingtin (mHTT) in microglia promoted cell-autonomous pro-inflammatory transcriptional activation by increasing the expression and transcriptional activities of the myeloid lineage-determining factors PU.1 and C/EBPs. We observed elevated levels of PU.1 and its target genes in the brains of mouse models and individuals with HD. Moreover, mHTT-expressing microglia exhibited an increased capacity to induce neuronal death *ex vivo* and *in vivo* in the presence of sterile inflammation. These findings suggest a cell-autonomous basis for enhanced microglia reactivity that may influence non-cell-autonomous HD pathogenesis.

Reactive microglia are associated with nearly all neurodegenerative diseases[1], but the mechanisms underlying microglia activation and their potential contributions to disease progression remain poorly understood. In contrast with Parkinson's and Alzheimer's diseases, which are related to a spectrum of genetic mutations and environmental factors[2,3], HD is a neurodegenerative disorder caused by specific expansion of a CAG repeat in the coding region of the *HTT* gene[4]. This mutation results in an elongated stretch of glutamine near the N terminus of HTT[4]. Polyglutamine expansions of more than 37 residues initiate a degenerative process that is characterized by the loss of medium spiny neurons in the striatum[5]. A number of roles of this protein have been uncovered, but the precise mechanism(s) by which mHTT causes dysfunction and degeneration of neurons remains an area of intense research.

Although HD is thought to be primarily caused by mutant protein expression in neurons, HTT is broadly expressed, including high levels of expression in microglia[6,7]. Despite the fact that microglia comprise <10% of the total brain cells[8], this specialized cell population rapidly responds to even minor pathological changes in the brain and may contribute directly to neuronal degeneration by producing an excess of various pro-inflammatory factors[9]. Several lines of evidence point to altered microglia activation states in the context of HD. Inflammation appears early in the onset of disease[10] and reactive microglia are conspicuous even in low-grade HD human brains, suggesting an early microglia response to changes in axons[11]. In patients' striatum and cortex, reactive microglia occur in all grades of pathology and accumulate in relation to the degree of neuronal loss[11]. Furthermore, an *in vivo* PET study showed that microglia activation correlates with the severity of the pathology in HD patients[12]. Substantial microglia activation in regions related to cognitive function in HD patients has recently been suggested to predict disease onset[13]. Monocytes from HD subjects express mHTT and have been reported to be hyperactive in response to stimulation[14]. A similar pattern was seen in macrophages and microglia derived from R6/2 (ref. 15) and YAC[14] HD mouse models. Notably, age-dependent changes in striatal microglial morphology and vasculature in the YAC128 mouse model of HD have been reported[16]. The cerebrospinal fluid and striatum of HD patients exhibit evidence of immune activation, with upregulation of IL6, IL8 and TNFα[14,17]. These cytokines can induce a CNS inflammatory response that alters the blood brain barrier and affects neuronal function[18], suggesting that they could contribute to disease progression. At a molecular level, dysfunctional kynurenine pathway[19], NFκB activation[20], cannabinoid receptor 2 signaling[21] and P2X7 receptor involvement[22] have been reported as potential mechanisms explaining HD inflammation in different mouse models.

Inflammation is normally an adaptive biological response to pathogen infection and tissue injury that serves to engage the immune system and tissue repair mechanisms. In these cases, inflammation resolves following eradication of the inciting stimulus. However, when pathological processes result in a sustained inflammatory response, persistent expression of mediators such as IL6, IL8 and TNFα can contribute to tissue damage and disease progression[23]. The observation of an inflammatory component of HD raises the question of whether inflammation is the response of surrounding cells to a

[1]Department of Cellular and Molecular Medicine, University of California, San Diego, La Jolla, California, USA. [2]Razavi Newman Integrative Genomics and Bioinformatics Core, Salk Institute for Biological Studies, La Jolla, California, USA. [3]Laboratory of Genetics, Salk Institute for Biological Studies, La Jolla, California, USA. [4]Department of Neurosciences, University of California, San Diego, La Jolla, California, USA. [5]Ludwig Institute for Cancer Research, La Jolla, California, USA. [6]Department of BioSciences and Center for Stem Cell Research, Università degli Studi di Milano, Milan, Italy. [7]Department of Medicine, University of California, La Jolla, San Diego, California, USA. Correspondence should be addressed to C.K.G. (ckg@ucsd.edu).

Received 31 October 2013; accepted 27 January 2014; published online 2 March 2014; doi:10.1038/nn.3668

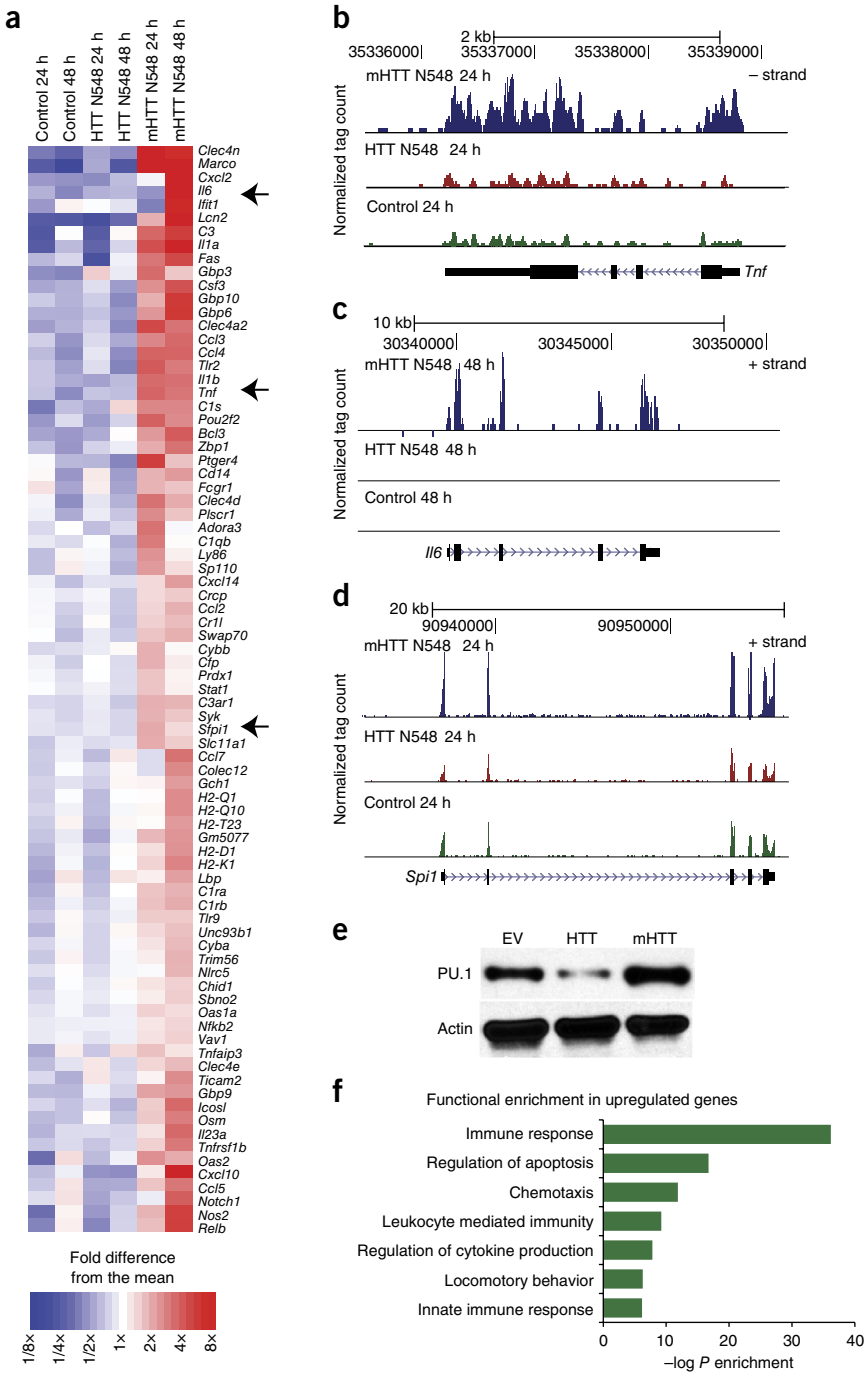

Figure 1 RNA-Seq analysis reveals that mHTT N terminus expression triggers pro-inflammatory gene expression in BV2 microglia. (**a**) Heat map representing RNA-Seq gene expression of upregulated inflammatory genes in BV2 microglia cell lines transduced with lentivirus expressing mHTT N548 in comparison with empty vector (control) and expressing HTT N548 at 24 and 48 h after plating. (**b**–**d**) UCSC Browser images representing normalized RNA-Seq read density from BV2 microglia cell lines transduced with empty vector (control), HTT N548 or mHTT N548 mapped at the *Tnf* **b**), *Il6* (**c**) and *Spi1* (*PU.1*) (**d**) genomic loci. (**e**) Western blots of PU.1 expression in BV2 microglia cell lines transduced with lentivirus empty vector (EV), HTT N548 or HTT N548 expression vectors. Shown is one representative experiment of three biological replicates. Full-length blot is presented in **Supplementary Figure 8**. (**f**) Gene Ontology analysis of functional annotations associated with upregulated genes in BV2 microglia expressing mHTT in comparison with wild-type HTT.

neuron-autonomous degenerative process and/or due to microglia-autonomous immune activation resulting from expression of mHTT. Regardless of the mechanism(s) responsible for microglia activation, the contribution of inflammation to HD pathogenesis remains poorly understood.

We investigated whether mHTT expression alters microglia function in a cell-autonomous fashion. Using genome-wide approaches, we found that mHTT expression in microglia resulted in increases in the expression of several inflammatory response genes even in the absence of pro-inflammatory stimuli. Unexpectedly, this phenomenon was linked to an increase in the expression and transcriptional activities of the myeloid lineage-determining factors PU.1 and C/EBPs. These transcription factors are required for the development and function of the macrophage/microglia lineage[9,23,24] and establish the regulatory potential of these cells by selecting enhancers and promoters that are acted on by signal-dependent transcription factors such as NFκB[24]. As a consequence of increased PU.1 and C/EBPs activity, mHTT-expressing microglia exhibited enhanced toxic effects on wild-type neurons in comparison with wild-type microglia *ex vivo* and after sterile inflammation *in vivo*.

RESULTS

mHTT promotes pro-inflammatory gene expression

To investigate potential cell-autonomous roles of mHTT in microglia, we generated isogenic BV2 microglia cell lines stably overexpressing the first 548 amino acids of the N terminus of human HTT or mHTT. These lines were maintained as pools of clones and cultured for 4 weeks before study to avoid acute effects of lentiviral infection on microglia activation. Deep sequencing revealed that microglia expressing mHTT N548 exhibited higher expression of mRNAs encoding pro-inflammatory factors as compared with cells expressing wild-type HTT N548 in the absence of pro-inflammatory stimulation (**Fig. 1a** and **Supplementary Table 1**). Notably, the increase in *Il6* and *Tnf* mRNA (**Fig. 1b**,**c**) was similar to the pattern previously observed in HD patients[14,17]. Expression of *Spi1* (encoding PU.1), a key factor in myeloid fate determination[9,24–26], was itself upregulated in the presence of mHTT N548 at the mRNA (**Fig. 1d**) and protein (**Fig. 1e**) levels. Conversely, in the presence of HTT N548, the expression of PU.1 was downregulated (**Fig. 1e**). Gene Ontology analysis of the entire set of upregulated genes, observed in presence of mHTT N548, indicated significant enrichment for terms related to innate immunity and inflammation ($P < 1 \times 10^{-15}$; **Fig. 1f**).

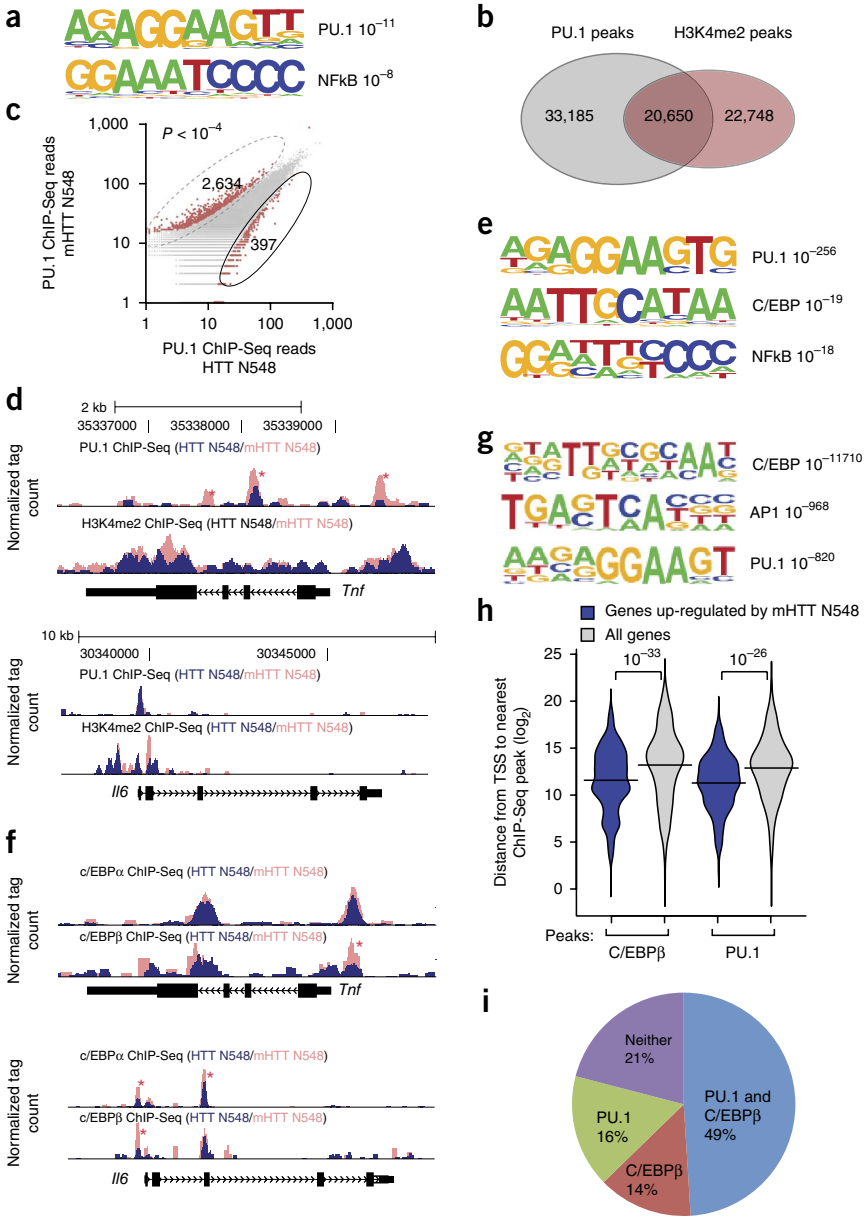

Figure 2 mHTT promotes pro-inflammatory gene expression via PU.1 and C/EBPs. (**a**) Motif enrichment in promoters of upregulated genes in BV2 microglia expressing mHTT N548 in comparison with HTT N548. (**b**) Venn diagram representing the overlap between PU.1 peaks and H3K4me2 peaks in BV2 cells expressing HTT N548 as detected by ChIP-Seq. (**c**) Scatter plot of normalized tag counts for PU.1 peaks detected in microglia cell lines overexpressing wild-type HTT versus mHTT (data points color-coded red indicate >4-fold difference, $P < 10^{-4}$). (**d**) PU.1 and H3K4me2 ChIP-Seq read density from BV2 microglia overexpressing wild-type HTT versus mHTT at the *Tnf* and *Il6* loci. Asterisks denote differential PU.1 binding. (**e**) Motif enrichment at PU.1 peaks specific for BV2 cells expressing mHTT N548. (**f**) C/EBPα and C/EBPβ ChIP-Seq read density from BV2 microglia overexpressing wild-type HTT versus mHTT at the *Tnf* and *Il6* loci. Asterisks denote differential C/EBP binding. (**g**) Motif enrichment at C/EBPβ peaks in BV2 cells expressing mHTT N548. (**h**) Distribution of distances from either mHTT N548 upregulated genes' promoters or all promoters to the nearest C/EBPβ and PU.1 ChIP-Seq peaks. (**i**) Pie diagram representing the fraction of genes upregulated by the presence of mHTT N548 with a C/EBPβ and/or PU.1 peak within 5 kb of the transcription start site (TSS).

To investigate potential mechanisms leading to the enhanced inflammatory gene expression in microglia expressing mHTT N548, we performed *de novo* motif enrichment analysis of transcriptional regulatory elements associated with the upregulated genes. Consistent with the upregulation of PU.1 expression, we observed a consensus PU.1 motif as the most enriched regulatory element in the enhancers and promoters of the upregulated genes in microglia cells expressing mHTT N548 (**Fig. 2a**). A binding motif for NFκB was the next most enriched motif, consistent with a previously described activation of this factor in presence of mHTT[20]. Given that PU.1 is a key factor in myeloid fate determination[9,25] and is required for selection of enhancers that are acted on by NFκB[24], these findings suggested a potential role of mHTT in priming myeloid cells toward inflammatory activation.

To establish a direct link between the increased expression of PU.1 and target genes, we performed chromatin immunoprecipitation coupled to deep sequencing (ChIP-Seq) to quantify PU.1 binding in BV2 microglia cells overexpressing either HTT N548 or mHTT N548. In addition, we performed ChIP-Seq analysis for H3K4me2, a histone modification associated with enhancers and promoters[27–29], thereby generating a microglia enhancer 'atlas'. In BV2 microglia expressing HTT N548, PU.1 was associated with approximately half of the H3K4me2-marked regions, consistent with the binding pattern of PU.1 in macrophages[24,30] (**Fig. 2b**). PU.1 peaks in microglia expressing HTT N548 or mHTT N548 largely overlapped, but mHTT N548 expression was associated with a significant number of differential PU.1 peaks (defined by a normalized tag count of >4-fold comparing mHTT N548 to HTT N548), consistent with the increased expression of PU.1 (2,634 differential sites in mHTT N548 cells versus 397 differential sites in HTT N548 cells, $P < 10^{-4}$; **Fig. 2c**).

Genomic loci encoding mRNAs that were upregulated in BV2 microglia expressing mHTT N548 generally exhibited higher enrichment of PU.1 binding to promoters and enhancers, exemplified by the *Tnf* locus (**Fig. 2d**). However, a subset of PU.1 target genes, exemplified by *Il6*, did not exhibit this pattern (**Fig. 2d**). This raised the question as to whether additional factors might cooperate with PU.1 to contribute to the observed upregulation of PU.1 target genes. *De novo* motif analysis of PU.1 binding sites in the vicinity of genes upregulated in the presence of mHTT N548 returned a motif for the C/EBP family of transcription factors (**Fig. 2e**). Members of the C/EBP family are required for myeloid cell development and induction of several inflammatory mediators[31,32]. To investigate a potential role of C/EBPs in contributing to expression of a subset of PU.1 target genes, we performed ChIP-Seq analysis for C/EBPα and C/EBPβ in BV2 microglia cells overexpressing HTT N548 or mHTT N548. Notably, we observed a stronger enrichment for C/EBPα and C/EBPβ on the *Il6* promoter/enhancer, as well as on *Tnf* promoter/enhancer, in mHTT

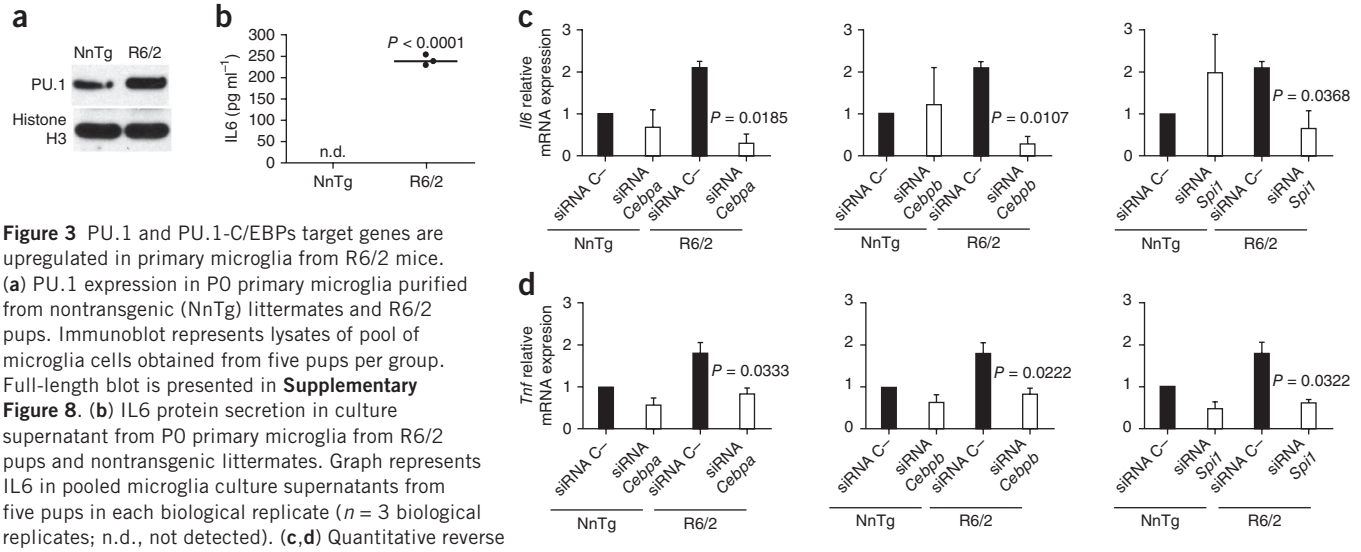

Figure 3 PU.1 and PU.1-C/EBPs target genes are upregulated in primary microglia from R6/2 mice. (**a**) PU.1 expression in P0 primary microglia purified from nontransgenic (NnTg) littermates and R6/2 pups. Immunoblot represents lysates of pool of microglia cells obtained from five pups per group. Full-length blot is presented in **Supplementary Figure 8**. (**b**) IL6 protein secretion in culture supernatant from P0 primary microglia from R6/2 pups and nontransgenic littermates. Graph represents IL6 in pooled microglia culture supernatants from five pups in each biological replicate ($n = 3$ biological replicates; n.d., not detected). (**c**,**d**) Quantitative reverse transcription PCR (qRT-PCR) analysis for *Il6* (**c**) and *Tnf* (**d**) mRNAs expression levels in the presence of *Cebpa*, *Cebpb* or *Spi1* siRNAs in nontransgenic littermates and R6/2 primary microglia (mean ± s.d., $n = 3$ biological replicates). siRNA C– is a nontargeting negative control. In all cases, *P* values were calculated using the two-tailed paired Student *t* test. Each experiment is representative of at least three independent replicates.

N548 cells (**Fig. 2f**). No differences in *Cebpa and Cebpb* mRNA expression levels were observed in microglia overexpressing wild-type or mHTT N548 (**Supplementary Table 1**). Motif enrichment analysis for C/EBPβ ChIP-Seq confirmed the correlation between this factor and PU.1 binding (**Fig. 2g**). Analysis of the correlation between the distance from promoter to the nearest C/EBPβ peak, as well as from promoter to the nearest PU.1 peak detected by ChIP-Seq and the altered gene expression in the presence of mHTT N548, indicated a higher correlation for C/EBPβ binding and PU.1 binding (10^{-33} and 10^{-26}, respectively) to induced genes in comparison with the total set of expressed genes (**Fig. 2h**). Nearly 80% of the upregulated genes in mHTT N548–expressing cells exhibited PU.1 and/or C/EBPβ binding within 5 kb of the transcriptional start site (**Fig. 2i**). In contrast, the corresponding frequency for all genes was ~51%. Together, these findings indicate a strong relationship of nearby PU.1 and C/EBPβ binding to upregulated genes in mHTT N548–expressing cells.

To confirm and extend the observations obtained from microglia cell lines overexpressing mHTT N548, we next measured the expression of *Spi1* (*PU.1*) and representative PU.1-C/EBPs target gene mRNAs in primary microglia derived from the R6/2 mouse model[33] expressing mHTT (exon 1), in the absence of pro-inflammatory stimulation. *Spi1* expression was significantly increased in primary microglia derived from newborn R6/2 mice, both at mRNA (+50% increase, $P < 0.0009$, two-tailed paired Student *t* test) and protein levels (**Fig. 3a**), in comparison with primary microglia from non-transgenic littermates. Corresponding increases were observed in the expression of *Il6* (threefold increase, $P = 0.0035$, two-tailed paired Student *t* test) and *Tnf* mRNAs (twofold increase, $P = 0.0075$, two-tailed paired Student *t* test). In contrast, increased expression of *Spi1*, *Il6* and *Tnf* was not observed in bone marrow–derived macrophages (BMDMs) from R6/2 mice (**Supplementary Fig. 1a–c**). We found no difference in *Cebpa* and *Cebpb* mRNA expression in primary microglia and BMDMs from R6/2 and nontransgenic littermates (data not shown). Thus, the observed increase of *Spi1* expression seems to be specific for primary microglia expressing mHTT (exon 1). Supernatants collected from the same R6/2 primary microglia cultures exhibited significantly increased ($P < 0.0001$) IL6 levels after 72 h of incubation, confirming the increased *Il6* mRNA expression observed in the same cells (**Fig. 3b**).

To investigate whether PU.1 and C/EBPα and C/EBPβ are required for controlling the enhanced pro-inflammatory gene expression that we observed in presence of mHTT (exon 1), we transfected primary microglia from R6/2 and non-transgenic littermates with specific siRNAs directed against *Cebpa*, *Cebpb* or *Spi1*. The three siRNAs effectively reduced the expression of their target mRNAs by ~80% in comparison with control siRNAs (**Supplementary Fig. 2**). Knockdown of *Cebpa*, *Cebpb* and *Spi1* separately greatly reduced the levels of mRNA expression of *Il6* and *Tnf* in primary microglia from R6/2 in comparison with microglia transfected with control siRNA (**Fig. 3c**,**d**). These data confirm the requirement of PU.1 and C/EBPs for increased expression of these pro-inflammatory mediators in cells expressing mHTT (exon 1) in the absence of pro-inflammatory stimulation.

mHTT promotes activation of microglia, but not BMDM

To extend these studies to a mouse model that is genetically analogous to human HD, we took advantage of a knock-in model characterized by a 175 CAG expansion in the *Htt* (*Hdh*) gene[34]. We evaluated *Spi1* mRNA and protein expression as well as the expression of representative PU.1-C/EBPs target genes in primary microglia derived from newborn (P0) wild-type, heterozygous and homozygous mHTT knock-in mice. We observed that *Spi1* was significantly upregulated in primary microglia from mice homozygous for mHTT (Q175/Q175), both at the mRNA and protein level (**Fig. 4a**), in comparison with wild-type HTT-expressing primary microglia cells (Q7/Q7). Consistently, mRNAs from PU.1-C/EBPs target genes *Il6*, *Tlr2* and *Irf1* were upregulated in primary microglia from homozygous mutant mice in the absence of pro-inflammatory stimulation (**Fig. 4b**). Furthermore, we performed RNA-Seq analysis of microglia derived from wild-type and knock-in $Hdh^{175/175}$ adult symptomatic mice. We verified that the expression of full-length mHTT *in vivo* in microglia was able to promote a genome-wide pro-inflammatory transcription signature similar to that observed in a microglia cell line expressing the N terminus fragment of mHTT (**Fig. 4c** and **Supplementary Table 2**).

Compatible with the observation of an increased activity of the myeloid lineage determining factors PU.1-C/EBPs, we also observed

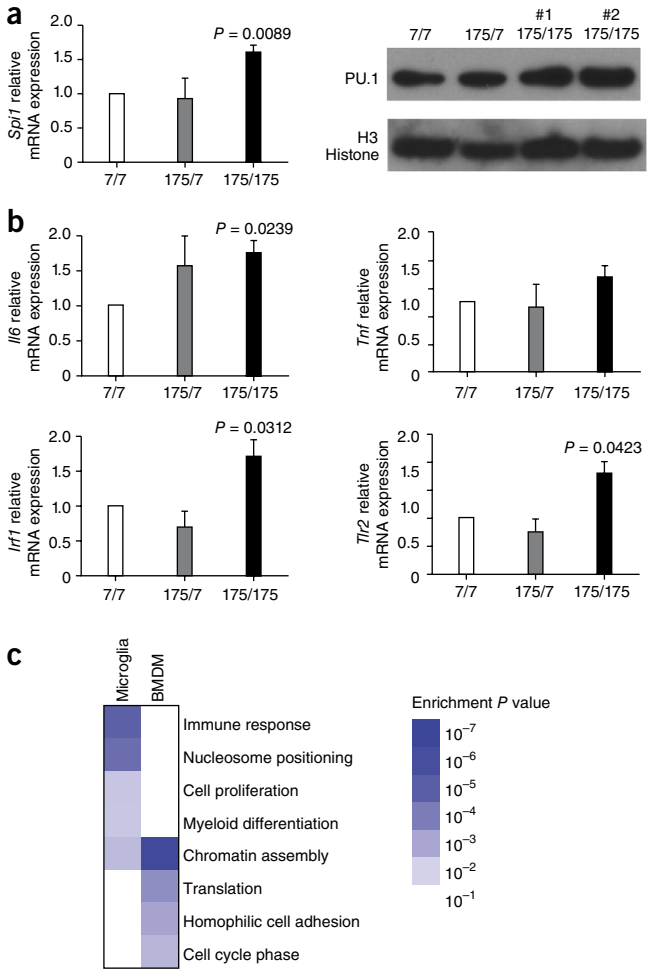

Figure 4 PU.1 and PU.1-C/EBPs target genes are upregulated in primary microglia from *Hdh*$^{175/175}$ knock-in mice. (**a**) qRT-PCR analysis for *Spi1* (*PU.1*) mRNA and protein expression in primary microglia purified from *Hdh*$^{7/7}$, *Hdh*$^{175/7}$ and *Hdh*$^{175/175}$ newborn (P0) pups (mean ± s.d., $n = 3$ biological replicates). Full-length blot is presented in **Supplementary Figure 8**. (**b**) qRT-PCR analysis for *Il6*, *Tnf*, *Irf1* and *Tlr2* mRNA expression in primary microglia purified from *Hdh*$^{7/7}$, *Hdh*$^{175/7}$ and *Hdh*$^{175/175}$ pups (mean ± s.d., $n = 3$ biological replicates). All *P* values were determined by two-tailed paired Student *t* test. (**c**) Gene Ontology analysis reporting the biological processes enriched in genes upregulated in *Hdh*$^{175/175}$ versus *Hdh*$^{7/7}$ microglia and BMDMs obtained from adult mice (18–20 months old). RNA-Seq results are based on mRNA extraction from pooled microglia cells or BMDMs obtained from four mice per group.

an enrichment for cell proliferation and myeloid differentiation genes in the GO analysis (**Fig. 4c**). Although the vast majority of HD patients only carry a single allele of mHTT, alterations in gene expression observed in microglia from homozygous *Hdh*$^{175/175}$ mice were less obvious in microglia from heterozygous mice. This finding suggests that genetic background, environmental factors, cellular context and age are important for determining penetrance of the mutant allele. Consistent with this, we performed RNA-Seq analysis of BMDMs obtained from the same mice (**Supplementary Table 2**). The analysis of the transcriptional profiles of BMDMs from wild-type and knock-in *Hdh*$^{175/175}$ mice revealed that the expression of Q175/Q175 did not produce the same pro-inflammatory transcriptional activation in BMDMs as we observed in microglia from the same mice (**Fig. 4c**), most likely reflecting both different origins[35,36] and environmental influences. As further proof of this, global RNA-Seq analysis of wild-type microglia and BMDMs clearly showed a substantial difference between the two myeloid cell populations in term of basal gene expression programs (**Supplementary Fig. 3**).

Pro-inflammatory transcription is specific for mHTT *in vivo*

To link the observations obtained *ex vivo* in primary microglia from different mouse models of HD with the disease progression *in vivo*, we evaluated the expression of *Spi1* and its pro-inflammatory target genes in adult R6/2 mice in comparison with non-transgenic littermates. Increased expression of *Spi1* mRNA was already evident in pre-symptomatic mice and was even greater at symptomatic stage in striatum from R6/2 mice (**Supplementary Fig. 4a**). Concomitantly, we detected an increase in the expression of *Il6*, *Tnf*, *Irf1* and *Tlr2* mRNA in the same region (**Supplementary Fig. 4b–e**). No difference in the levels of *Cebpa* or *Cebpb* mRNA expression was observed in striatum from R6/2 and nontransgenic littermates (data not shown). The levels of *Spi1* expression as well as the pro-inflammatory gene expression correlated with the disease progression in the R6/2 model of HD. In parallel, we analyzed the expression of PU.1 and specific PU.1– C/EBPα and C/EBPβ target pro-inflammatory genes in spinal cord, cortex and striatum of SOD1^{G37R} mice, an animal model for amyotrophic lateral sclerosis (ALS)[37]. ALS is also a progressive neurodegenerative disease that primarily affects motor neurons that connect the brain and spinal cord to muscles, resulting in a fatal paralysis a few years after onset[38]. Even though microglia activation is important for ALS pathogenesis[39], PU.1 and specific PU.1– C/EBPα and C/EBPβ target pro-inflammatory genes that were elevated in mutant Huntingtin models were not increased in striatum, cortex or spinal cord from 1-year-old symptomatic SOD1^{G37R} mice (**Supplementary Fig. 5a–e**). These results are consistent with a specific, cell-autonomous role of mHTT in promoting basal activation of pro-inflammatory genes via the lineage-determining factors PU.1, C/EBPα and C/EBPβ.

Enhanced pro-inflammatory transcription in HD brains

We next investigated the expression of *SPI1* (*PU.1*), *CEBPA* and *CEBPB*, as well as their targets in striatum, cortex and monocytes from human HD and control individuals. *SPI1* expression was increased in striatal as well as in cortical post-mortem human samples from HD individuals, in concert with increased levels of *IL6*, *IRF1* and *TLR2* mRNAs in the striatum and a trend increase of *IL6*, *TNF* and *TLR2* in the cortex of the HD individuals (**Fig. 5a–c** and **Supplementary Fig. 6a,b**). No changes in *CEBPA* and *CEBPB* mRNAs levels were detected in cortical or striatal samples from HD individuals in comparison with matching controls (data not shown). The expression of *SPI1*, *CEBPA* and *CEBPB*, as well as their target genes, showed no substantial difference in monocytes from HD patients (**Fig. 5a–c** and **Supplementary Fig. 6a,b**). These observations confirm and extend the distinct inflammatory profile that has been observed in post-mortem HD brains[14,17]. We next performed immunostaining for PU.1 in frontal cortex as well as in striatum of five frozen post-mortem samples from HD individuals and matching controls (**Fig. 5d**). We observed an increase in the number of microglia per section (**Fig. 5d**), consistent with previous observations[11]. Quantification of the intensity and distribution of PU.1 staining further revealed a significant increase in PU.1 expression on a per cell basis (~2-fold, $P = 0.018$ in the striatum and ~2-fold, $P = 0.0013$ in the cortex; **Fig. 5e**). These *in vivo* findings in the brains of patients with HD are therefore consistent with what we observed in primary microglia expressing mHTT isolated from two different rodent models as well as in BV2 microglia expressing mHTT N548.

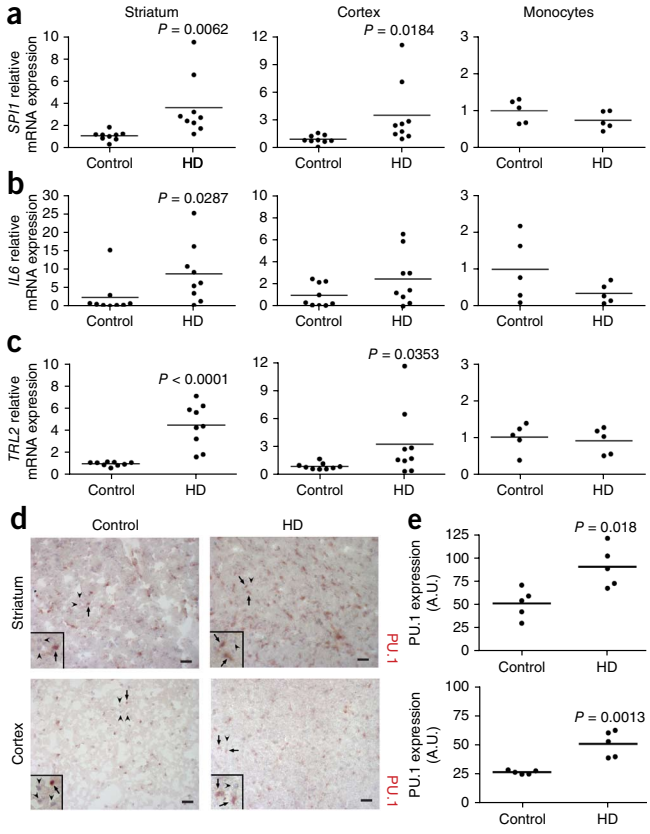

Figure 5 Inflammation *in vivo* in HD individuals. (**a**–**c**) qRT-PCR analysis for *SPI1* (**a**), *IL6* (**b**) and *TLR2* (**c**) mRNA expression in striatum (first column, $n = 9$ individual specimen per group), cortex (second column, $n = 9$ individual specimen per group) and monocytes (third column, $n = 5$ individual specimen per group) from controls and HD individuals (Vonsattel grade 3 and 4). Each dot is representative of one individual. All *P* values were determined by unpaired Student *t* test. (**d**) PU.1 immunohistochemistry staining on post-mortem frozen samples of striatum (caudate/putamen) and cortex (Brodmann area 4) from HD ($n = 5$, Vonsattel grade 3) and matching controls ($n = 5$). One representative picture is shown for each group. (**e**) Densitometric analysis of PU.1 staining. Each dot is representative of PU.1 expression of one individual ($n = 5$ individual specimen per group). Arbitrary unit (A.U.) is defined by the number of pixels representing the area of PU.1 staining normalized by the number of PU.1$^+$ microglia cells. PU.1$^+$ microglia cells were distinguished morphologically from endothelial cells. All *P* values were determined by unpaired Student *t* test. Scale bars represent 100 µm. Insets highlight PU.1$^+$ cells. Arrows in representative pictures and insets for each condition point to PU.1$^+$ nuclei, arrowheads point to PU.1$^-$ nuclei.

Effect of mHTT microglia on neurons *ex vivo* and *in vivo*

Experiments using neuron and glia co-culture *in vitro* suggest that activation of innate immunity in the CNS can trigger neuronal death[40]. We recently reported that reduced Nurr1 expression results in exaggerated inflammatory responses in microglia, leading to the production of factors that cause death of tyrosine hydroxylase–expressing neurons[41]. Given that we observed exaggerated IL6 secretion by mHTT (exon 1)–expressing microglia (**Fig. 3b**), we investigated whether neuron-microglia co-culture would exhibit any neurotoxic effects of microglia expressing mHTT on wild-type neurons. This possibility was evaluated by co-culturing mouse embryonic stem cell–derived normal neurons over a substrate of wild-type primary astrocytes. Subsequently, wild-type (Q7/Q7) or mHTT knock-in microglia (Q175/Q175) cells were added to the culture. The addition of mHTT-expressing microglia, but not wild-type microglia, increased neuronal apoptosis (**Fig. 6a**).

To extend these observations *in vivo*, we considered the possibility that sterile inflammation could be triggered in HD patients by endogenous molecules, such as DAMPs, components of dead neurons and protein aggregates. As a means of mimicking sterile inflammation, we performed stereotactic injection of lipopolysaccharide (LPS) into the striatum of 12–15-week-old wild-type or *Hdh*$^{175/175}$ mice. Given the fact that LPS mainly triggers microglia activation, but has no direct toxic effect on neurons[40], LPS-induced neurotoxicity is secondary to microglia activation. No difference was detected in the number of degenerating neurons in wild-type versus *Hdh*$^{175/175}$ mice injected with saline solution as measured by Fluoro-Jade B staining. This result is consistent with the lack of HD symptoms or CNS pathology in *Hdh*$^{175/175}$ mice at this age[42]. In contrast, LPS induced greater neuronal death in *Hdh*$^{175/175}$ mice than in wild-type mice (**Fig. 6b**). As a negative control, no Fluoro-Jade B$^+$ cells were detected in the contralateral non-injected hemispheres. This result is consistent with exaggerated inflammatory and neurotoxic responses of microglia expressing mHTT, but does not exclude the possibility that this was also a result of increased sensitivity of neurons expressing mHTT. To directly address this concern, we mated a mouse expressing the

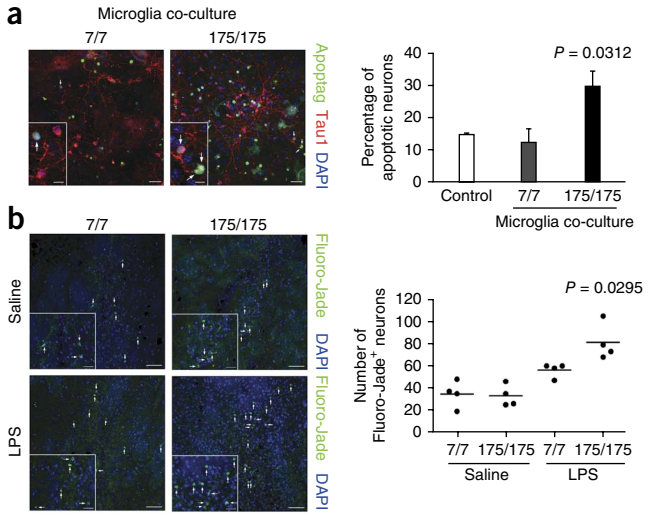

Figure 6 Effect of mHTT-expressing microglia on primary neurons *ex vivo* and *in vivo*. (**a**) TUNNEL assay for neuron, astrocyte and microglia co-culture in the presence of primary microglia from wild-type *Hdh*$^{7/7}$ or homozygous mHTT knock-in mice (*Hdh*$^{175/175}$). Arrows in representative pictures for each condition point to apoptotic neurons. Insets highlight TUNEL-positive neurons. Scale bars represent 30 µm and 10 µm (insets). Quantitative representation of the percentage of Apoptag$^+$ neurons, obtained by the ratio between the number of triple-positive cells (Apoptag$^+$, TAU1$^+$ and DAPI$^+$ cells)/ total number of double-positive (TAU1$^+$ and DAPI$^+$) cells (mean ± s.d., $n = 3$ biological replicates), with pools of microglia from four pups per group. Control represents neurons and astrocytes co-cultured without microglia added. *P* value was determined by one-tailed paired Student *t* test. (**b**) Fluoro-Jade B staining of coronal brain sections from wild-type (*Hdh*$^{7/7}$) or homozygous mHTT knock-in mice (*Hdh*$^{175/175}$) injected with saline solution or LPS (5 µg). One representative image for each condition is shown (left). Arrows in representative pictures and insets for each condition point to Fluoro-Jade B$^+$ neurons. Scale bars represent 50 µm and 20 µm (insets). Quantitative representation of the number of Fluoro-Jade B$^+$ degenerated/dead neurons (right). Each dot represents the number of Fluoro-Jade B$^+$ neurons per mouse ($n = 4$ mice per group, one-way ANOVA and Tukey's *post hoc* test).

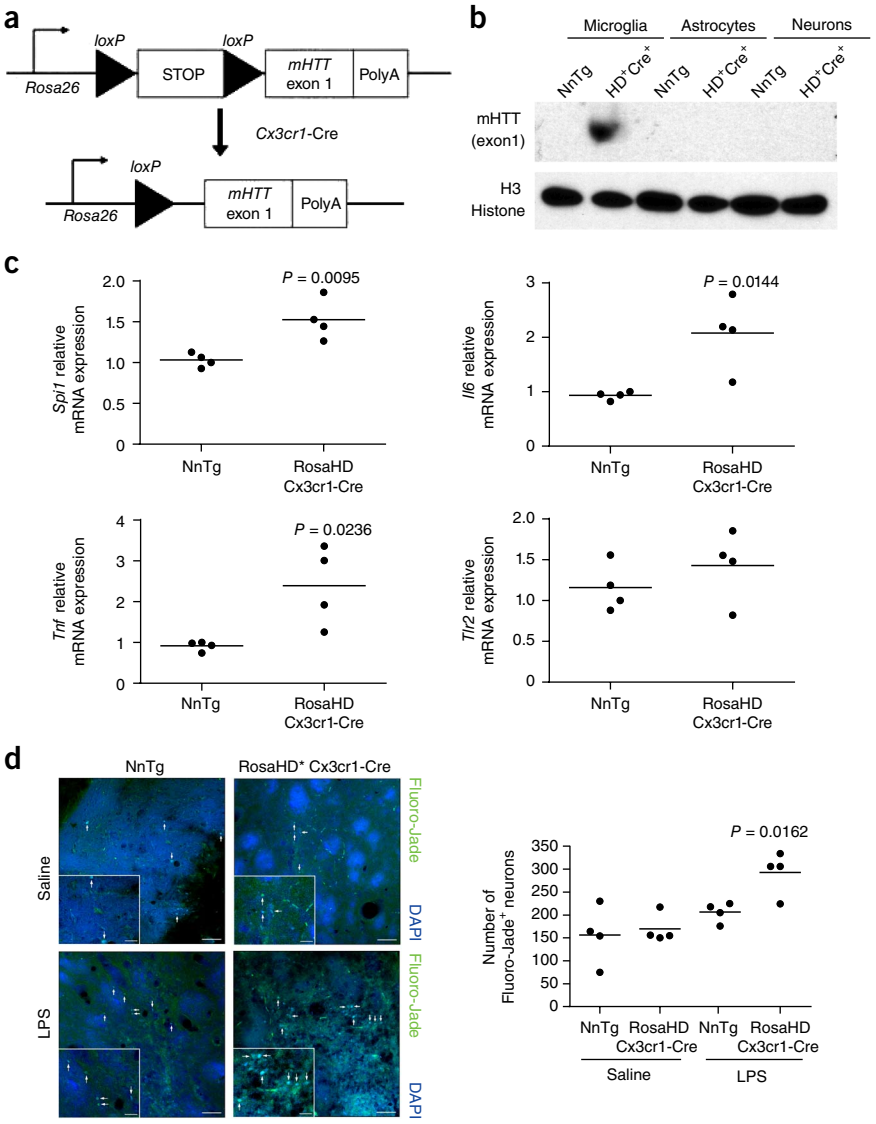

Figure 7 Effect of mHTT-expressing microglia on wild-type neurons *in vivo*. (**a**) The schematics of conditional HD mice in which expression of mHTT (exon 1) was dependent on the expression of *Cx3cr1*-driven Cre recombinase. *mHTT* (exon 1) was targeted to the Rosa26 locus. The targeted locus contained the endogenous *Rosa26* promoter, a transcriptional STOP sequence, two *loxP* sites (black triangles), *mHTT* exon 1 with 103 mixed CAA-CAG repeats (encoding a polyglutamine expansion) and a polyadenylation signal (PolyA). (**b**) mHTT (exon 1) protein expression in primary microglia, astrocytes and neurons purified from RosaHD$^+$ × Cx3cr1-Cre$^+$ and nontransgenic littermates. Immunoblot represents lysates of pool of microglia, astrocytes and neurons obtained from four pups per group. Full-length blot is presented in **Supplementary Figure 8**. (**c**) qRT-PCR analysis for *Spi1*, *Il6*, *Tnf* and *Tlr2* mRNAs expression in striatum from 8-week-old nontransgenic littermates and RosaHD × Cx3cr1-Cre mice. Each dot is representative of one mouse. All *P* values were determined by unpaired Student *t* test ($n = 4$ mice per group). (**d**) Fluoro-Jade B staining of coronal brain sections from nontransgenic littermates or RosaHD × Cx3cr1-Cre mice injected with saline solution or LPS (5 μg). One representative image for each condition is shown (left). Arrows in representative pictures and insets for each condition point to Fluoro-Jade B$^+$ neurons. Scale bars represent 50 μm and 20 μm (insets). Quantitative representation of the number of Fluoro-Jade B$^+$ degenerated/dead neurons (right). Each dot represents the number of Fluoro-Jade B$^+$ neurons per mouse ($n = 4$ mice per group, one-way ANOVA and Tukey's *post hoc* test).

myeloid-specific Cre driver (Cx3cr1-Cre) to RosaHD knock-in mice[43] (**Fig. 7a**), which resulted in exclusive microglia-specific expression of mHTT (exon 1) in the brain (**Fig. 7b**). Expression of the mHTT (exon 1) in microglia was sufficient to induce an increase in the transcription of *Spi1*, *Il6* and *Tnf* mRNAs in the striatum of RosaHD × Cx3cr1-Cre mice in comparison with nontransgenic littermates (**Fig. 7c**). We used these and control mice to determine whether expression of mHTT (exon 1) selectively in microglia among brain cells results in exaggerated neuronal death following an inflammatory insult. We performed stereotactic injection of LPS into the striatum of 8-week-old RosaHD × Cx3cr1-Cre and nontransgenic littermates mice. We found that mice expressing mHTT (exon 1) in microglia showed an enhanced incidence of neuronal death in the presence of sterile inflammation in comparison with nontransgenic littermates (**Fig. 7d**). Taken together, these results demonstrate a potential contribution of microglia activation and inflammation to HD pathogenesis.

DISCUSSION

Previous studies of the inflammatory component of HD have provided evidence for alterations of signal-dependent mechanisms in the brains of HD mouse models, including NFκB activation[20], cannabinoid receptor 2 signaling[21] and P2X7 receptor involvement[22]. We found that the expression of mHTT specifically in microglia was sufficient to confer a cell-autonomous increase in pro-inflammatory gene expression and exaggerated neurotoxic effects on wild-type neurons *ex vivo* and after pro-inflammatory stimulation *in vivo*. Several lines of evidence support a mechanism in which mHTT exerts a cell-autonomous effect in microglia by increasing the expression and transcriptional activities of the myeloid lineage-determining factors PU.1, C/EBPα and C/EBPβ. Binding sites for PU.1 and C/EBPs were highly enriched in enhancers and promoters associated with the genes exhibiting constitutive upregulation in mHTT-expressing microglia. Expression of PU.1 itself was increased at both the mRNA and protein levels in mHTT-expressing microglia, and ChIP-Seq analysis demonstrated enhanced binding of PU.1 at thousands of genomic locations in these cells. Increased binding of PU.1 was associated with enhanced co-occupancy by C/EBPs, and the combination of enhanced PU.1 and C/EBP binding was highly correlated with increased expression of nearby genes, such as *Il6* and *Tnf*. Furthermore, given that PU.1, C/EBPα and C/EBPβ are lineage-determining factors, we could speculate that their increased activity in mHTT-expressing microglia and the concomitant enrichment for cell proliferation and myeloid differentiation genes in the GO analysis could be implicated in the increased density of microglia observed in HD individuals[11].

Recent studies have suggested that PU.1, C/EBPs and AP-1 proteins function in a collaborative manner to select a large fraction of the

functional enhancers in the macrophage that are acted on by signal-dependent transcription factors[26] (**Supplementary Fig. 7**). Of particular relevance to our findings, increased expression of a conditional form of PU.1 resulted in a coordinate increase in PU.1, C/EBPα and C/EBPβ binding throughout the genome, without changes in C/EBPα and C/EBPβ expression[26]. Our previous studies demonstrated that enhancers selected by PU.1 and C/EBPs provide access to signal-dependent factors such as nuclear receptors and NFκB, providing the basis for cell-specific responses[26]. Our findings are therefore consistent with a model in which mHTT-induced PU.1 expression drives the selection PU.1-C/EBPs–dependent enhancers that promote expression of pro-inflammatory/neurotoxic mediators in microglia under basal conditions (**Supplementary Fig. 7**). Eventually, sterile inflammation triggered in HD patients by endogenous molecules, such as components of dead neurons and protein aggregates, could lead to a further microglia activation and result in an increased neuronal death (**Supplementary Fig. 7**). This mechanism would explain both increases in basal gene expression and enhanced responses to exogenous stimuli and suggests a molecular basis for the state of priming defined recently on the basis of morphological evidence[16].

Our findings are consistent with the possibility that exaggerated microglia activation could contribute to the early inflammatory reaction observed in HD[11,16,44]. In particular, we observed that primary microglia derived from R6/2 mice constitutively express and secrete increased amounts of the pro-inflammatory cytokine IL6. Although a previous study did not find evidence for IL6 secretion by microglia from R6/2 mice in absence of stimulation[14], this apparent discrepancy with our data can easily be explained by the fact that we used a more sensitive detection system than that used in the previous study. Our results provide a potential explanation for previous observations of increased IL6 in the cerebrospinal fluid of HD patients before the clinical onset of disease[45]. Moreover, it has been suggested that microglia can modulate adult neurogenesis, such as when activated by inflammation[46]. IL6 appears to be one of the key mediators of this anti-neurogenic effect[47]. This abnormal IL6 secretion, reported here and by others[14,17], could also help to explain the impaired neurogenesis that has been reported in several mouse models of HD[48–50].

In addition to conferring a cell-autonomous basal increase in expression of pro-inflammatory and neurotoxic mediators, our findings suggest that expression of mHTT in microglia also confers increased sensitivity to extrinsic inducers of inflammation. Because microglia are the primary cells capable of responding to LPS in the brain parenchyma, the observation that *Hdh*$^{175/175}$ mice exhibited increased neuronal apoptosis following LPS injection is consistent with exaggerated neurotoxic responses of *Hdh*$^{175/175}$ microglia on wild-type neurons *ex vivo*. The *in vivo* observation from *Hdh*$^{175/175}$ mice could be explained in part by the fact that neurons expressing mHTT are more fragile than normal neurons and therefore more sensitive to the toxic effect induced by mHTT microglia. In our opinion, the *in vivo* experiment might reflect what could happen in HD patients, where cell-autonomous microglia hyper-activation coupled with neuronal fragility can concur to promote disease progression. Nevertheless, the experiment conducted on mice expressing mHTT (exon 1) in microglia clearly showed that microglia activation in HD is sufficient to promote neuronal degeneration and can have a potential contribution to the pathogenesis of the disease. However, further studies will be required to establish whether selective expression of mHTT in microglia is sufficient to exert neuropathological and behavioral deficits in mice.

In the context of HD, what seems to be a general transcriptional mechanism underlying macrophage and possibly microglia activation appears to be specifically related to the expression of mHTT exclusively in microglia. In fact, the PU.1-C/EBPs–dependent enhanced basal pro-inflammatory genes expression was not observed in the CNS of an animal model for ALS carrying a mutation in the *Sod1* gene. This result is particularly relevant considering that ALS is a progressive neurodegenerative disease in which microglia activation has a key role in pathogenesis[39]

Notably, the effects of mHTT on PU.1-dependent programs of gene expression appeared to be microglia specific, as we found no differences in PU.1 levels or pro-inflammatory gene expression in BMDMs obtained from R6/2 and *Hdh*$^{175/175}$ mice or monocytes from HD individuals. The basis for specific effects of mHTT on microglia gene expression is unclear, but recent lineage tracing experiments provide evidence that microglia are derived from fetal yolk sac progenitors very early in development and represent a self-renewing population of cells that is independent of BMDMs[35,41]. It is therefore possible that either this unique origin or the specific differentiation program conferred by residence in the CNS determines the cell-autonomous functions of mHTT in microglia. Collectively, our findings reveal a previously unknown and unexpected role of mHTT in disrupting the regulation of microglia identity and function and provide further impetus to better understand the contribution of microglia activation to the pathogenesis of HD.

METHODS

Methods and any associated references are available in the online version of the paper.

Accession codes. All ChIP-Seq and RNA-Seq data sets have been deposited in the NCBI GEO database under accession number GSE54443.

Note: Any Supplementary Information and Source Data files are available in the online version of the paper.

ACKNOWLEDGMENTS

We thank E. Mejia for Fluoro-Jade B staining, H. Kordasiewicz (ISIS Pharmaceuticals) for providing R6/2 mice, M. McAlonis, J. Artates and J. Boubaker for stereotaxic injection, University of California at San Diego (UCSD) Histology Core for PU.1 staining, the UCSD Human Embryonic Stem Cell Core Facility at Sanford Consortium for Regenerative Medicine for assistance with cell sorting, J. Corey-Bloom (Shiley-Marcos Alzheimer's Disease Research Center) for providing blood samples from HD patients, M. Hayden (University of British Columbia) for providing HTT and mHTT N548 aa original cDNA, S. Georges for assistance in quantification of TUNNEL assay, the Harvard Brain Tissue Resource Center (supported in part by PHS R24 MH068855), New York Brain Bank at Columbia University and Massachusetts General Hospital for HD post-mortem samples. C.L.T. and D.W.C. are supported by the CHDI Foundation. These studies were supported by US National Institutes of Health grants DK091183, DK063491, GM 069338 and CA17390 to C.K.G.

AUTHOR CONTRIBUTIONS

C.K.G. and A.C. developed the study, conceived the experimental plans and analyzed the data. C.B. analyzed the genome-wide data. A.C. performed most of the biological, biochemical and molecular experiments. B.E.K. conceived and performed the TUNNEL assay experiment. D.G. performed microglia purification from adult mice brains. C.L.-T. provided *Hdh*$^{175/175}$ SOD1^{G37R} tissues, mice and performed the *in vivo* experiment. E.C. and C.Z. participated in the elaboration of the project and provided original constructs and mRNA from post-mortem human samples. D.W.C. and F.H.G. participated in experimental design and provided essential resources and reagents. C.K.G. and A.C. interpreted the data and wrote the manuscript. All of the authors read and edited the manuscript. C.K.G. supervised the entire work, directed the strategies, provided financial support and gave final approval of the manuscript.

COMPETING FINANCIAL INTERESTS
The authors declare no competing financial interests.

1. Streit, W.J., Walter, S.A. & Pennell, N.A. Reactive microgliosis. *Prog. Neurobiol.* **57**, 563–581 (1999).
2. Samii, A., Nutt, J.G. & Ransom, B.R. Parkinson's disease. *Lancet* **363**, 1783–1793 (2004).
3. Schellenberg, G.D. & Montine, T.J. The genetics and neuropathology of Alzheimer's disease. *Acta Neuropathol.* **124**, 305–323 (2012).
4. The Huntington's Disease Collaborative Research Group. A novel gene containing a trinucleotide repeat that is expanded and unstable on Huntington's disease chromosomes. *Cell* **72**, 971–983 (1993).
5. Reiner, A. *et al.* Differential loss of striatal projection neurons in Huntington disease. *Proc. Natl. Acad. Sci. USA* **85**, 5733–5737 (1988).
6. Ferrante, R.J. *et al.* Heterogeneous topographic and cellular distribution of huntingtin expression in the normal human neostriatum. *J. Neurosci.* **17**, 3052–3063 (1997).
7. Trottier, Y. *et al.* Cellular localization of the Huntington's disease protein and discrimination of the normal and mutated form. *Nat. Genet.* **10**, 104–110 (1995).
8. Lawson, L.J., Perry, V.H., Dri, P. & Gordon, S. Heterogeneity in the distribution and morphology of microglia in the normal adult mouse brain. *Neuroscience* **39**, 151–170 (1990).
9. Kierdorf, K. *et al.* Microglia emerge from erythromyeloid precursors via Pu.1- and Irf8-dependent pathways. *Nat. Neurosci.* **16**, 273–280 (2013).
10. Tai, Y.F. *et al.* Microglial activation in presymptomatic Huntington's disease gene carriers. *Brain* **130**, 1759–1766 (2007).
11. Sapp, E. *et al.* Early and progressive accumulation of reactive microglia in the Huntington disease brain. *J. Neuropathol. Exp. Neurol.* **60**, 161–172 (2001).
12. Pavese, N. *et al.* Microglial activation correlates with severity in Huntington disease: a clinical and PET study. *Neurology* **66**, 1638–1643 (2006).
13. Politis, M. *et al.* Microglial activation in regions related to cognitive function predicts disease onset in Huntington's disease: a multimodal imaging study. *Hum. Brain Mapp.* **32**, 258–270 (2011).
14. Björkqvist, M. *et al.* A novel pathogenic pathway of immune activation detectable before clinical onset in Huntington's disease. *J. Exp. Med.* **205**, 1869–1877 (2008).
15. Crocker, S.F., Costain, W.J. & Robertson, H.A. DNA microarray analysis of striatal gene expression in symptomatic transgenic Huntington's mice (R6/2) reveals neuroinflammation and insulin associations. *Brain Res.* **1088**, 176–186 (2006).
16. Franciosi, S. *et al.* Age-dependent neurovascular abnormalities and altered microglial morphology in the YAC128 mouse model of Huntington disease. *Neurobiol. Dis.* **45**, 438–449 (2012).
17. Silvestroni, A., Faull, R.L., Strand, A.D. & Moller, T. Distinct neuroinflammatory profile in post-mortem human Huntington's disease. *Neuroreport* **20**, 1098–1103 (2009).
18. van Gool, W.A., van de Beek, D. & Eikelenboom, P. Systemic infection and delirium: when cytokines and acetylcholine collide. *Lancet* **375**, 773–775 (2010).
19. Giorgini, F., Guidetti, P., Nguyen, Q., Bennett, S.C. & Muchowski, P.J. A genomic screen in yeast implicates kynurenine 3-monooxygenase as a therapeutic target for Huntington disease. *Nat. Genet.* **37**, 526–531 (2005).
20. Khoshnan, A. *et al.* Activation of the IkappaB kinase complex and nuclear factor-kappaB contributes to mutant huntingtin neurotoxicity. *J. Neurosci.* **24**, 7999–8008 (2004).
21. Palazuelos, J. *et al.* Microglial CB2 cannabinoid receptors are neuroprotective in Huntington's disease excitotoxicity. *Brain* **132**, 3152–3164 (2009).
22. Díaz-Hernández, M. *et al.* Altered P2X7-receptor level and function in mouse models of Huntington's disease and therapeutic efficacy of antagonist administration. *FASEB J.* **23**, 1893–1906 (2009).
23. Medzhitov, R. Inflammation 2010: new adventures of an old flame. *Cell* **140**, 771–776 (2010).
24. Heinz, S. *et al.* Simple combinations of lineage-determining transcription factors prime cis-regulatory elements required for macrophage and B cell identities. *Mol. Cell* **38**, 576–589 (2010).
25. Bonifer, C., Hoogenkamp, M., Krysinska, H. & Tagoh, H. How transcription factors program chromatin–lessons from studies of the regulation of myeloid-specific genes. *Semin. Immunol.* **20**, 257–263 (2008).
26. Walsh, J.C. *et al.* Cooperative and antagonistic interplay between PU.1 and GATA-2 in the specification of myeloid cell fates. *Immunity* **17**, 665–676 (2002).
27. Chepelev, I., Wei, G., Wangsa, D., Tang, Q. & Zhao, K. Characterization of genome-wide enhancer-promoter interactions reveals co-expression of interacting genes and modes of higher order chromatin organization. *Cell Res.* **22**, 490–503 (2012).
28. Brykczynska, U. *et al.* Repressive and active histone methylation mark distinct promoters in human and mouse spermatozoa. *Nat. Struct. Mol. Biol.* **17**, 679–687 (2010).
29. Regha, K. *et al.* Active and repressive chromatin are interspersed without spreading in an imprinted gene cluster in the mammalian genome. *Mol. Cell* **27**, 353–366 (2007).
30. Ghisletti, S. *et al.* Identification and characterization of enhancers controlling the inflammatory gene expression program in macrophages. *Immunity* **32**, 317–328 (2010).
31. Tsukada, J., Yoshida, Y., Kominato, Y. & Auron, P.E. The CCAAT/enhancer (C/EBP) family of basic-leucine zipper (bZIP) transcription factors is a multifaceted highly-regulated system for gene regulation. *Cytokine* **54**, 6–19 (2011).
32. Huber, R., Pietsch, D., Panterodt, T. & Brand, K. Regulation of C/EBPbeta and resulting functions in cells of the monocytic lineage. *Cell. Signal.* **24**, 1287–1296 (2012).
33. Mangiarini, L. *et al.* Exon 1 of the HD gene with an expanded CAG repeat is sufficient to cause a progressive neurological phenotype in transgenic mice. *Cell* **87**, 493–506 (1996).
34. Heikkinen, T. *et al.* Characterization of neurophysiological and behavioral changes, MRI brain volumetry and 1H MRS in zQ175 knock-in mouse model of Huntington's disease. *PLoS ONE* **7**, e50717 (2012).
35. Ginhoux, F. *et al.* Fate mapping analysis reveals that adult microglia derive from primitive macrophages. *Science* **330**, 841–845 (2010).
36. Schulz, C. *et al.* A lineage of myeloid cells independent of Myb and hematopoietic stem cells. *Science* **336**, 86–90 (2012).
37. Wong, P.C. *et al.* An adverse property of a familial ALS-linked SOD1 mutation causes motor neuron disease characterized by vacuolar degeneration of mitochondria. *Neuron* **14**, 1105–1116 (1995).
38. Boillée, S., Vande Velde, C. & Cleveland, D.W. ALS: a disease of motor neurons and their nonneuronal neighbors. *Neuron* **52**, 39–59 (2006).
39. Boillée, S. *et al.* Onset and progression in inherited ALS determined by motor neurons and microglia. *Science* **312**, 1389–1392 (2006).
40. Lehnardt, S. *et al.* Activation of innate immunity in the CNS triggers neurodegeneration through a Toll-like receptor 4–dependent pathway. *Proc. Natl. Acad. Sci. USA* **100**, 8514–8519 (2003).
41. Saijo, K. *et al.* A Nurr1/CoREST pathway in microglia and astrocytes protects dopaminergic neurons from inflammation-induced death. *Cell* **137**, 47–59 (2009).
42. Menalled, L.B. *et al.* Comprehensive behavioral and molecular characterization of a new knock-in mouse model of Huntington's Disease: zQ175. *PLoS ONE* **7**, e49838 (2012).
43. Gu, X. *et al.* Pathological cell-cell interactions elicited by a neuropathogenic form of mutant Huntingtin contribute to cortical pathogenesis in HD mice. *Neuron* **46**, 433–444 (2005).
44. Kraft, A.D., Kaltenbach, L.S., Lo, D.C. & Harry, G.J. Activated microglia proliferate at neurites of mutant huntingtin-expressing neurons. *Neurobiol. Aging* **33**, 17–33 (2012).
45. Björkqvist, M. *et al.* A novel pathogenic pathway of immune activation detectable before clinical onset in Huntington's disease. *J. Exp. Med.* **205**, 1869–1877 (2008).
46. Battista, D., Ferrari, C.C., Gage, F.H. & Pitossi, F.J. Neurogenic niche modulation by activated microglia: transforming growth factor beta increases neurogenesis in the adult dentate gyrus. *Eur. J. Neurosci.* **23**, 83–93 (2006).
47. Monje, M.L., Toda, H. & Palmer, T.D. Inflammatory blockade restores adult hippocampal neurogenesis. *Science* **302**, 1760–1765 (2003).
48. Ransome, M.I. & Hannan, A.J. Impaired basal and running-induced hippocampal neurogenesis coincides with reduced Akt signaling in adult R6/1 HD mice. *Mol. Cell. Neurosci.* **54**, 93–107 (2013).
49. Simpson, J.M. *et al.* Altered adult hippocampal neurogenesis in the YAC128 transgenic mouse model of Huntington disease. *Neurobiol. Dis.* **41**, 249–260 (2011).
50. Kohl, Z. *et al.* Impaired adult olfactory bulb neurogenesis in the R6/2 mouse model of Huntington's disease. *BMC Neurosci.* References for On-line Methods. **11**, 114 (2010).

ONLINE METHODS

Ethics statement. This study was performed in strict accordance with the recommendations in the Guide for the Care and Use of Laboratory Animals of the US National Institutes of Health. The protocol was approved by the Institutional Animal Care and Use Committee of UCSD and every effort was made to minimize suffering. Studies of human brain samples were performed without individually identifiable information. Research undertaken on such specimens did not meet the regulatory definition of human subjects research.

Human samples. Autopsy brain samples from control and HD patients were provided to E.C. from the archives of the Harvard Brain Bank Tissue Resource Center (Ct 6002, Ct 5919, Ct 5074, Ct 5021, AN13574, AN13112, AN08704, AN15088, AN10090, AN09667, HD 6010, HD 5570, HD 6062, HD 6062, AN06034, AN14935, AN13326, AN18743, AN10094, AN15530, AN13238, AN07121, AN04187, AN14307, AN10314, AN12699, AN13041, AN17896, AN08666, AN01077), from New York Brain Bank at Columbia University (Ct-T99, Ct T-168), and from Massachusetts General Hospital (HD 3723, HD 3484). Control subjects were matched to HD patients for sex and age. All diagnoses were based on clinical assessment and histopathological evaluation by experienced neuropathologists according to Vonsattel classification. Fresh blood samples were obtained from J. Corey-Bloom at Shiley-Marcos Alzheimer's Disease Research Center: 7135, 7150, 7151, 7152, 7153, 6000, 6018, 7082, 7094, 7129.

Cell lines. Murine microglial BV2 cells, primary mouse microglia and mouse astrocytes were maintained with DMEM (Cellgro) supplemented with 10% (vol/vol) fetal bovine serum (FBS, low endotoxin, Hyclone) and penicillin/streptomycin (Invitrogen).

Mice and isolation of primary cells. C57BL/6, R6/2 and RosaHD[43] mice were purchased from Jackson Lab. Tg(Cx3cr1-cre)MW126Gsat mice were generated by N. Heintz (The Rockefeller University, GENSAT) and purchased from MMRRC (UC Davis), and together with *Hdh*$^{Q175/Q175}$ and SOD1^{G37R} mice housed according to UCSD protocols. mHTT (exon 1) expression has been verified by Western Blot on microglia, astrocytes and neurons cells lysates obtained from RosaHD^{+} × Cx3cr1-Cre^{+} and nontransgenic littermates. Primary microglia cells and astrocytes have been purified from the cerebrum of P0 pups. After 10–14 days of culture, microglia cells were isolated from astrocytes as described previously[41]. Primary neurons were purified from mice cerebrum using Papain Dissociation System (LKL003153, Worthington) according to manufacturer's instructions. BMDMs were obtained from adult mice as previously reported[24]. Human monocytes have been purified from freshly collected blood samples by Ficoll-Plaque and selected using Pan Monocytes Isolation Kit (Miltenyi, #130-096-537) according to manufacturer's instructions.

Reagents. N terminus human wild-type and N terminus mHTT were cloned from pCAG-Htt19550-15Q and pCAG-Htt1955-128Q, respectively, into MCS of pCDH-CMV-MCS-EF1-Puro (System Bioscience) using EcoRI and NotI. Lentiviral production and BV2 cells transduction were performed according to the manufacturer's protocol. Control cell line was generated by transducing BV2 cells with lentivirus obtained from pCDH-CMV-MCS-EF1-Puro (empty vector). Validation of plasmids used in this study was performed by western blotting.

SiRNA for C/EBPα sequence: 5′-ACAACAUCGCGGUGCGCAAUU-3′. SiRNAs for C/EBPβ, PU.1 and siGENOME non-targeting were purchased from Thermo Scientific (ON-TARGETplus SMART pool 043110, 041420 and 001210, respectively) and was transfected in primary mouse microglia by Lipofectamin 2000 (Invitrogen) according with manufacturer's instructions.

Adult microglia purification. Mice were deeply anesthetized and then perfused intracardially with ice-cold DPBS (Mediatech 21-031CV). Cortex, striatum and hippocampus were extracted and gently homogenized in staining buffer (HBSS (Life Technologies, 14175-095), 1% (wt/vol) BSA, 1 mM EDTA) on ice using a 2-ml polytetrafluoroethylene pestle (Wheaton), first in a 14-ml round-bottom tube (BD Falcon, 352059) and then in a 2-ml grinder chamber (Wheaton, 358029). Homogenates were filtered onto a 70-µm cell strainer (BD Falcon, 352350) and centrifuged for 10 min at 400 *g*. Cell pellets were resuspended in 6 ml of 37% isotonic Percoll (Sigma, P4937) and then underlaid with 5 ml of 70% isotonic Percoll in a 15-ml centrifuge tube (Corning, 430790). Tubes were then centrifuged at 600 *g* for 40 min at 18 °C, with no acceleration or deceleration. Cells at the 37–70% Percoll interface were recovered and washed once in 15 ml HBSS. Cell were then incubated in staining buffer on ice with CD16/CD32 (eBioscience, clone 93) antibody for 25 min, and then with CD11b-PE (BioLegend 101208, clone M1/70) and CD45-Alexa488 (BioLegend 103122, clone 3-F11) antibodies for 30 min. Cells were then washed once and filtered onto a 40-µm cell strainer (BD Falcon, 352340). Sorting was performed on a BD Influx cell sorter. Microglia were defined as singlets, CD11b^{+} CD45^{Low} events, and encompassed 90–95% of all CD11b^{+} events.

Microglia and embryonic stem cell (ESC)-derived neuron co-culture. Mouse E14 ESCs were maintained on gelatin-coated dishes in ES medium (Glasgow Minimum Essential Medium, Sigma G5154) supplemented with 15% FBS (Atlanta Biologicals), 2 mM L-glutamine (Gibco), 1× non-essential amino acids (Gibco), 1× sodium pyruvate (Gibco), 55 µM of 2-mercaptoethanol (Gibco) and 1,000 U ml^{-1} LIF (Millipore), as described previously[51]. Neural progenitor cells were generated and differentiated as described previously[52]. ESCs were grown in suspension in ES medium without LIF for the first day and in N2/B27 medium (DMEM/F12-Glutamax Medium (Gibco) supplemented with 1× B27 (Gibco) and 1× N2 (Gibco) supplements) supplemented with 500 ng ml^{-1} Noggin (PeproTech) for four more days. Next, embryoid bodies were dissociated, plated on and maintained on laminin-coated dishes in N2/B27 medium supplemented with 20 ng ml^{-1} EGF (PeproTech), 20 ng ml^{-1} FGF2 (Stemgent), and 10 µg ml^{-1} heparin (Sigma). Neural progenitor cells were differentiated into neurons in N2/B27 medium supplemented with 500 µg ml^{-1} cAMP (Sigma), 0.2 µM ascorbic acid (Sigma), 20 ng ml^{-1} BDNF (R&D), and 20 ng ml^{-1} GDNF (R&D) at least for 5 d before starting a co-culture with primary mouse astrocytes and medium was supplemented with 2% FBS (Hyclone). Primary microglia were plated on neuron-astrocyte co-cultures at 30,000 cells. Microglia triple co-cultures were maintained for another 24 h before proceeding with immunohistochemistry.

TUNEL staining and quantification. Cells were fixed with 4% paraformaldehyde (wt/vol) in phosphate-buffered saline (PBS) for 15 min, blocked and permeabilized with donkey serum (10%, vol/vol) and Triton X-100 (0.1%, vol/vol) in PBS and were incubated overnight with mouse monoclonal TAU1 (1:250, Covance). Next day, cells were incubated with secondary antibodies against mouse and 1 µg ml^{-1} DAPI. TUNEL staining was performed using ApopTag Fluorescein Direct *In situ* Apoptosis Detection Kit (Millipore) as described by the manufacturer. Briefly, cells were post-fixed in cooled ethanol:acetic acid (2:1) and incubated with TdT enzyme at 37 °C for 1h. For quantification, epifluorescence images for 20 random fields were taken using Stereo Investigator Software (MBF Biosciences) and number of DAPI^{+} nuclei, TAU1^{+} neurons and TUNEL^{+} apoptotic neurons were counted using ImageJ (US National Institutes of Health). The number of apoptotic neurons has been obtained by the ratio between the number of triple-positive cells (Apoptag^{+}, TAU1^{+} and DAPI^{+} cells)/ total number of double-positive TAU1^{+} and DAPI^{+} cells. At both steps researchers were blind to the experimental conditions.

Stereotaxic injection of LPS in the mouse striatum *in vivo*. Mice (12–15 weeks of age for *Hdh*$^{Q7/Q7}$ and *Hdh*$^{Q175/Q175}$ or 8 weeks of age for RosaHD × Cx3cr1-Cre and nontransgenic littermates) were anesthetized using a mixture of ketamine/xylazine (100 mg per kg, 10 mg per kg) and immobilized in a stereotaxic apparatus. The stereotaxic injection site into the right striatum was AP +0.9 mm, ML +2.25 mm, DV −3 mm from bregma. A stainless steel cannula (5-µl Hamilton syringe) was inserted and a single 1-µl injection of 5 µg of LPS (Sigma) or 1 µl of PBS was delivered over a 2-min period into the same coordinates.

Immunofluorescence and quantification. 1 week after injection, experimental animals were anesthetized and perfused transcardially with 0.9% (wt/vol) saline followed by 4% paraformaldehyde. The brain samples were post-fixed with 4% paraformaldehyde overnight and equilibrated in 30% (wt/vol) sucrose. Coronal sections of 40 µm were prepared with a sliding microtome and stored in cryoprotectant (ethyleneglycol, glycerol, 0.1 M phosphate buffer pH 7.4, 1:1:2 by volume) at −20 °C. IHC and co-labeling immunofluorescence for free-floating sections were performed with Fluoro-Jade B (Chemicon, #AG310) as follows. Tissue sections were mounted onto gelatinized slides and allowed to dry at 25 °C. Slides were immersed in ethanol solution at different descending concentrations and H_2O all

doi:10.1038/nn.3668

for 1 min each. Then, slides were incubated in 0.06% $KMnO_4$ (wt/vol) for 5 min and washed in H_2O for 1 min. Fluoro-Jade B (liquid stock solution, 0.01%, wt/vol) was added to the slides and left to incubate for 30 min. Finally, after washing and drying overnight, slides were immersed in Neoclear and mounted on coverslip. 4,6-diamidino-2-phenylindole (DAPI, 1:1,000, Roche) was used to reveal nuclei. In the case of wild-type and *Hdh*$^{175/175}$ mice experiment, to determine the number of Fluoro-Jade B$^+$ degenerated/dead neurons, the number of double-positive cells (Fluoro-Jade B$^+$ and DAPI$^+$) were counted in six contiguous sections per mouse. In the case of RosaHD × Cx3cr1-Cre and nontransgenic littermates experiment, massive cell death was observed after LPS injection for both genotypes. Thus, to determine the number of Fluoro-Jade B$^+$ degenerated/dead neurons, the number of double-positive cells (Fluoro-Jade B$^+$ and DAPI$^+$) as well as the green puncta clusters within/surrounding DAPI nuclei were counted as positive in nine contiguous sections per each mouse. Scoring was performed by an investigator who was blind to the experimental conditions.

Immunohistochemistry (IHC) and quantification. Post-mortem frozen brain samples (Brodmann area 4, caudate-putamen) were cryosectioned at 5 microns and used in the immunohistochemistry assays. Controls included sections of human spleen (control for macrophages), rabbit IgG (negative control), diluting buffer (1% BSA in PBS) and rabbit anti-Von Willebrand factor (blood vessel marker, positive control). Each step of the assay was followed by buffer rinses. Endogenous peroxidase was blocked with 0.03% (vol/vol) H_2O_2 (Fisher # H325-100) for 30 min. Endogenous collagen was blocked with 1% BSA/PBS (Sigma #A4503G) for 30 min. Sections were fixed with 10% (vol/vol) neutral-buffered formalin (Fisher SF93-4) for 30 min, washed with PBS and overlaid with either rabbit IgG (1:100, Dako #N1699) or rabbit antibody to PU.1 (1:100, Cell Signaling #2266S) overnight in a humid chamber at 4 °C. Binding was detected using horseradish peroxidase–labeled antibody to rabbit (Jackson #111-035-144) at 1:500 for 30 min at 25 °C. Substrate color development was performed using the AEC kit (Vectorlab #H 5501). Nuclei were counterstained using Mayer's hematoxylin and slides were aqueous mounted for viewing and digital photomicrography using an Olympus BH2 microscope, equipped with a digital Magnafire camera. For quantification, five images for each sample were captured. To determine the intensity of signal, the number of pixels representing the area of PU.1 staining was calculated automatically using Magic Wand Tool (Adobe Photoshop). For each image, the number of PU.1+ microglia cells is represented by the number of noncontiguous areas in which PU.1 staining merging nuclear staining automatically revealed by the software. PU.1+ microglia cells were distinguished morphologically from endothelial cells.

RNA isolation and quantitative PCR. Total RNA was isolated by RNeasy kit (Qiagen) from BV2 cells, microglia, monocytes and BMDMs. Cortex and striatum from R6/2, SOD1^{G37R}, RosaHD × Cx3cr1-Cre mice as well as HD post-mortem brain samples were processed with Trizol (Invitrogen) to extract total RNA. 1 µg of total RNA was used for cDNA synthesis using Superscript III (Invitrogen), and quantitative PCR was performed with SYBR-GreenER (Invitrogen) detected by 7300 Real Time PCR System (ABI). The sequences of qPCR primers used for mRNA quantification in this study were obtained from PrimerBank[53]. For human samples, the results were normalized over expressed Alu repeats[54].

Western blotting. BV2 cells, primary microglia, astrocytes and neurons were lysed with buffer C (150 mM NaCl, 250 mM Tris HCl pH 7.5, 1% Triton X-100, 10% (vol/vol) glycerol, 5 mM EDTA, 1 mM EGTA) plus 1 mM PMSF, 1 mM DTT, Complete Protease Inhibitor Cocktail (Roche). Lysates were incubated in ice for 1 h. Finally, lysates were cleared by spinning at 4 °C at 13,000 rpm for 10 min. The protein concentrations in the supernatants were then determined using the BCA protein assay (Bio-Rad) as described by the manufacturers. A total of 100 µg of protein was separated by SDS-polyacrylamide electrophoresis using NuPAGE 4–12% bis-tris gel (Invitrogen), then transferred electrophoretically to a PVDF membrane. The membranes were blocked by incubation with 5% non-fat milk (wt/vol) in Tris-buffered saline containing 0.1% Tween-20 (vol/vol) (TBST) for 60 min at 25 °C. The membranes were then incubated overnight at 4 °C with primary antibody to PU.1 (1:1,000, sc-352, Santa Cruz), antibody to actin (1:10,000, CP01, Calbiochem), antibody to Histone H3 (1:1,000, Cell Signaling, #4620) and antibody to Polyglutamine (1:500, MAB1574, Millipore). The membranes were washed in TBST (3 × 5 min) before a 1-h incubation with peroxidase-linked secondary antibodies to rabbit or mouse accordingly at 25 °C. The immunoblots were then visualized using the enhanced chemiluminescence method (Amersham).

ELISA for IL6. IL6 quantification in cell culture supernatant have been performed with Mouse Interleukin-6 (IL6) ELISA kit from Thermo Scientific, according to manufacturer's instructions.

Chromatin immunoprecipitation (ChIP). ChIP was performed as described previously[24]. Briefly, 20x10^6 cells were crosslinked in 1% formaldehyde/PBS for 10 min at 25 °C. After quenching the reaction by adding 125 mM glycine, we washed the cells twice with PBS and centrifuged them (8 min, 800 *g*, 4 °C). Cells were resuspended in swelling buffer (10 mM HEPES/KOH pH 7.9, 85 mM KCl, 1 mM EDTA, 0.5% (vol/vol) IGEPAL CA-630 by volume, 1× protease inhibitor cocktail (Roche), 1 mM PMSF) for 5 min. Cells were spun down and resuspended in 500 µl of lysis buffer (50 mM Tris-HCl pH 7.4, 1% SDS, 0.5% (vol/vol) EmpigenBB, 10 mM EDTA, 1× protease inhibitor cocktail (Roche), 1 mM PMSF) and chromatin was sheared to an average DNA size of 300–400 bp by administering five pulses of 10-s duration at 10-W power output with 30-s pause on ice using a Misonix 3000 sonicator. The lysate was cleared by centrifugation (5 min, 16,000 *g*, 4 °C), and supernatant was diluted 2.5-fold with 750-µl dilution buffer (20 mM Tris-HCl pH 7.4, 100 mM NaCl, 0.5% Triton X-100, 2 mM EDTA, 1× protease inhibitor cocktail; Roche). The diluted lysate was pre-cleared by rotating for 2 h at 4 °C with 120 µl 50% rProtein A Sepharose Fast Flow (GE Healthcare). The beads were discarded, and 1% of the supernatant was kept as ChIP input. The protein of interest was immunoprecipitated by rotating the supernatant with 2.5 µg antibody overnight at 4 °C, then adding 50 µl blocked rProtein A Sepharose and rotating the sample for an additional 1 h at 4 °C. The beads were pelleted (2 min, 1,000 *g*, 4 °C), the supernatant discarded, and the beads were transferred in 400 µl of wash buffer I (WBI: 20 mM Tris-HCl pH 7.4, 150 mM NaCl, 0.1% SDS, 1% Triton X-100, 2 mM EDTA) into 0.45-µm filter cartridges (Ultrafree MC, Millipore), spun dry (1 min, 2,200*g*, 4 °C), washed one more time with WBI, and twice each with WBII (20 mM Tris-HCl pH 7.4, 500 mM NaCl, 1% Triton X-100, 2 mM EDTA), WBIII (10 mM Tris-HCl pH 7.4, 250 mM LiCl, 1% IGEPAL CA-630, 1% (wt/vol) sodium deoxycholate, 1 mM EDTA), and TE. Immunoprecipitated chromatin was eluted twice with 100 µl of elution buffer each (100 mM $NaHCO_3$, 1% SDS) into fresh tubes for 20 min. Eluates were pooled, the Na^+ concentration was adjusted to 300 mM with 5 M NaCl and crosslinks were reversed overnight at 65 °C in a hybridization oven. The samples were sequentially incubated at 37 °C for 2 h each with 0.33 mg ml^{-1} RNase A and 0.5 mg ml^{-1} proteinase K. The DNA was isolated using the QiaQuick PCR purification kit (Qiagen) according to the manufacturer's instructions. We used antibodies to PU.1 (sc-352), C/EBPα (sc-61), C/EBPβ (sc-150), control rabbit IgG (sc-2027) (Santa Cruz Biotech), H3K4me2 (cat#07-030, Millipore). For all antibodies, the working dilution was 1:1,000.

RNA sequencing. RNA was purified using RNeasy Mini Kit (Qiagen) and enriched for Poly(A)-RNA with MicroPoly(A) Purist Kit (Ambion). Subsequently, RNA was treated with TURBO DNase (Ambion), fragmented with RNA Fragmentation Reagents (Ambion) and purified by a P-30 column (Bio-Rad). Fragmented RNA was dephosphorylated with Antarctic phosphatase (New England Biolabs) heat inactivated and precipitated over-night. Poly(A)-tailing and cDNA synthesis was performed as previously described[55]. For reverse transcription, oligonucleotides with custom barcodes (underlined, slashes represent the four different bar codes) were used: 5′-Phos-CA/TG/AC/GT.GATCGTCGGACTGTAGAACTCT/idSp/CAAGCAGAAGACGGCATACGATTTTTTTTTTTTTTTTTTTVN-3′, where idSp represents the internal spacer 1′2′-dideoxyribose (dSpacer). Subsequently, exonuclease was used to remove the excess oligonucleotide. After heat inactivation, RNA was hydrolyzed by alkaline treatment (100 mM NaOH) and heat at 95 °C for 25 min. The cDNA fragments of 50–150 nucleotides were purified on a denaturing Novex 10% polyacrylamide TBE-urea gel (Invitrogen). The recovered cDNA was circularized, linearized, amplified for 12 cycles, and gel purified as previously described[55]. The library was sequenced on the Illumina HiSeq 2000 according to the manufacturer's instructions. Reads were aligned to the mouse mm9 genome (NCBI Build 37) using Tophat. RNA-Seq experiments were normalized and visualized using HOMER (http://homer.salk.edu/homer/) to generate custom tracks for the UCSC Genome Browser (http://genome.ucsc.edu/).

Gene expression values were generating for RefSeq annotated transcripts using HOMER and differential expression calculations were performed using edgeR[27]. Gene Ontology analysis was performed using DAVID (http://david.abcc.ncifcrf.gov/). Gene expression clustering was performed using Cluster 3.0 and visualized using Java TreeView. Promoters of regulated genes were analyzed for enriched motifs using HOMER[24].

ChIP-sequencing and data analysis. DNA from chromatin immunoprecipitation (10–50 ng) was adaptor-ligated and PCR amplified according to the manufacturer's protocol (Illumina). ChIP fragments were sequenced for 36 or 50 cycles on an Illumina HiSeq 2000 according to the manufacturer's instructions. Reads were aligned to the mouse mm9 genome assembly (NCBI Build 37) using Bowtie allowing up to two mismatches. Only tags that mapped uniquely to the genome were considered for further analysis. ChIP-Seq experiments were normalized and visualized by using HOMER (http://homer.salk.edu/homer/) to generate custom tracks for the UCSC Genome Browser (http://genome.ucsc.edu/). Peak finding, motif finding, and peak annotation were performed using HOMER. Peaks were assigned to gene targets based on the closest RefSeq defined TSS. Randomizations were performed during the HOMER motif finding algorithm. These involved selecting random fragments of genomic DNA to be used as control regions for motif discovery. Randomly selected fragments of DNA were selected to normalize GC% content.

Statistical analyses. Standard deviation and Student's *t* test and one-way ANOVA were performed with the Prism 4 program. $P < 0.05$ was considered significant. Unpaired *t* test was used for comparisons between control and transgenic mice within one group and between control and HD samples. Data are presented as mean ± s.d. For each experiment, a minimum sample size of three biological replicates was analyzed in each experimental condition. No statistical methods were used to pre-determine sample sizes, but our sample sizes are similar to those generally employed in the field. The estimate of the variance within each group was calculated and found to be similar between groups that were being statistically compared.

51. Gaspard, N. *et al.* Generation of cortical neurons from mouse embryonic stem cells. *Nat. Protoc.* **4**, 1454–1463 (2009).
52. Marchetto, M.C. *et al.* Non-cell-autonomous effect of human SOD1 G37R astrocytes on motor neurons derived from human embryonic stem cells. *Cell Stem Cell* **3**, 649–657 (2008).
53. Wang, X. & Seed, B. A PCR primer bank for quantitative gene expression analysis. *Nucleic Acids Res.* **31**, e154 (2003).
54. Marullo, M. *et al.* Expressed Alu repeats as a novel, reliable tool for normalization of real-time quantitative RT-PCR data. *Genome Biol.* **11**, R9 (2010).
55. Ingolia, N.T., Ghaemmaghami, S., Newman, J.R. & Weissman, J.S. Genome-wide analysis *in vivo* of translation with nucleotide resolution using ribosome profiling. *Science* **324**, 218–223 (2009).

doi:10.1038/nn.3668